American Mineralogist, Volume 91, pages 1747–1760, 2006

Thermal diffusivity of olivine-group minerals at high temperature

MAIK PERTERMANN* AND ANNE M. HOFMEISTER

Department of Earth and Planetary Sciences, Washington University, Campus box 1169, 1 Brookings Drive, St. Louis, Missouri 63130-4899, U.S.A.

ABSTRACT

Thermal diffusivity (D) data from 12 oriented single crystals and seven polycrystalline samples of olivine group minerals were acquired with the laser-flash method at temperatures (T) of up to ~1500 °C. Samples included forsterite, Fe-Mg binary olivines, sinhalite, and chrysoberyl; specimens were characterized using infrared spectroscopy and electron microprobe analysis. Crystal orientation and chemistry both affect D. For our single crystals, $D_{[100]} > D_{[001]} > D_{[010]}$ at all temperatures. Thermal diffusivity decreases with increasing T and becomes virtually constant at high temperatures. At room temperature, $D_{[001]}$ of pure forsterite has the highest observed values, but substitution of a small amount of Co in forsterite (0.3 wt% CoO) lowers D by ~20%. Substitution of ~10% Fe for Mg in forsterite, as in typical mantle olivine, lowers D by ~50%. At room temperature, mantle olivine has D = 3.25, 1.66, and 2.59 mm^2/s for the [100], [010], and [001] orientations, respectively. The values decrease to 0.93–0.87 mm^2/s at 790–985 °C for [100], 0.54–51 mm^2/s at 590–740 °C for [010] and 0.83–0.79 mm^2/s at 740–890 °C for [001]. Two dunite samples have D of 0.55–0.56 mm^2/s at 890–1080 °C, showing the effect of preferred orientation of grains dominated by [010]. Thermal diffusivity of polycrystalline samples is controlled by the large amounts of olivine present; minor phases offset the curves for $D(T)$ from the value of the olivine mineral. Our laser-flash measurements isolate the phonon component of heat transfer from radiative transfer and show that the phonon contribution becomes nearly constant for the high temperatures expected in the mantle. The other microscopic component (diffusive radiative transfer) depends strongly on temperature and this temperature dependence likely exerts greater control on mantle convection.

Keywords: New technique, laser-flash method, high-temperature studies, thermal diffusivity of olivine, olivine-group minerals

INTRODUCTION

Olivine is a major constituent mineral of Earth's upper mantle and oceanic crust and is thus of great geological and geophysical significance. To comprehend thermal regimes in Earth's upper mantle and their evolution with time, it is essential to understand olivine's heat transfer properties. For example, variable thermal properties influence the temperature distribution in subducting slabs, which in turn can affect the stability of olivine near the transition zone and occurrence of deep earthquakes (Hauck et al. 1999; Branlund et al. 2000). Also, thermal properties of olivine influence the temperature distribution in the upper mantle and its convection patterns (Dubuffet et al. 1999, 2000; Honda and Yuen 2001; Van den Berg et al. 2002).

Numerous studies of heat transfer by *phonons* (lattice diffusivity or conductivity) in mantle olivine exist (e.g., Katsura 1995; Osako et al. 2004; Xu et al. 2004), but nevertheless, significant discrepancies remain with respect to the temperature dependence (Hofmeister 1999) and absolute values of thermal diffusivity (D) for mantle minerals (Gibert et al. 2003a). Earlier thermal diffusivity measurements of olivine (e.g., Kanamori et al. 1968; Kobayashi 1974; Gibert et al. 2003a) showed a strong correlation of D with crystal orientation and chemistry, but disagreements occur even between the room-temperature measurements (e.g., see Gibert et al. 2003a), and disparities increase with temperature. Many of the previous studies were limited to olivine compositions near Fo_{90} [forsterite content, molecular Mg/(Mg + Fe)·100].

Questions regarding transport of *phonons* in olivines largely stem from simultaneous movement of heat in the experiments by *photon*s; radiative transfer (D_{rad}) is difficult to comprehend because it consists of two different processes and is also frequency dependent. The diffusive type of radiative transfer is calculated using spectroscopic measurements under various assumptions (Shankland et al. 1979; Hofmeister 1999, 2005). Purely diffusive radiative transfer occurs in the mantle due to the short distances (cm) that light is extinguished by scattering and absorption compared to the long distances over which temperature is nearly constant (km). Radiative transfer in experiments contains a direct component (also known as boundary-to-boundary or ballistic radiative transfer) as even centimeter-sized samples allow some frequencies of light to cross the entire sample without being significantly attenuated. That two different processes operate in the Earth and in the laboratory should be obvious from the temperature gradients, which exceed 1 K/mm = 10^6 K/km in the laboratory but are merely 10 K/km in mantle boundary layers. Gibert et al. (2005) and Höfer and Schilling (2002) assumed that both types of radiative transport (boundary-to-boundary and diffusive) exist in experiments. The results of Gibert et al. (2005) for D of the lattice component (D_{lat}) of olivine depend on each of the approximations used to evaluate these two distinct types of

* Present address: Department of Earth Science, Rice University, Houston, Texas 77005. E-mail: Maik.Pertermann@rice.edu

radiative transfer. The effect of direct radiative transfer on their measurements is modeled using a finite difference approach by assuming that the rear surface receives light in proportion to the emitted heat inferred from measurements of temperature near the front surface of the sample (Höfer and Schilling 2002; Schilling 1999). Radiative transfer effects not removed by this approach are assumed to be diffusive. However, it is highly unlikely that the diffusive type is present in the experiments because at the temperatures investigated the blackbody peak overlaps the transparent near-infrared region of the olivine spectrum. At the frequencies where the most light is produced, little attenuation occurs in centimeter-sized olivine samples, as evidenced by near-IR data at temperature in Hofmeister (2005). To the best of our knowledge, the finite difference model apparently does not incorporate the dependence of sample absorption on frequency and temperature (Gibert et al. 2005). Because absorbance changes with temperature, this approach potentially contributes an error to the temperature derivative of D. In all probability, such modeling incompletely removes boundary-to-boundary radiative transfer.

In addition, the extraction of diffusive radiative transfer from experiments, once direct transfer is accounted for, involves assuming forms for each of the phonon and photon components [e.g., Gibert et al. (2005) assumed $D_{lat} = 1/(A + BT)$ and $D_{rad} = CT^3$]. However, the T^3 law (Clark 1957) is the form derived for thermal conductivity ($k = \rho C_P D$, where ρ is density and C_P is heat capacity), *not* thermal *diffusivity*; and at the temperatures where the fitting is performed, C_P depends on T. Moreover, the T^3 form is inappropriate for minerals in general and for Fe^{2+} bearing olivine because it was derived assuming constant, non-zero absorbance over all frequencies and all temperatures (Shankland et al. 1979; Hofmeister 2005). This is certainly not the case for olivine as shown by spectroscopic measurements (e.g., Shankland et al. 1979; Taran and Langer 2001; Ullrich et al. 2002). The fact that Gibert et al. (2003a, 2005) observe direct radiative transfer in their raw data (temperature-time curves) proves that their sample is optically thin, which violates the conditions needed for radiative transfer to be diffusive, and definitively shows that their experiments cannot be governed by Clark's T^3 formulation.

It is also debatable whether the form $D_{lat} = 1/(A + BT)$ is universally correct. This form has been justified on the basis of experimental data (e.g., Seipold 1998). However, for the fitting to be valid, experiments would need to be devoid of radiative transfer of either type. From Figure 3 of Gibert et al. (2005), radiative transport is significant in some measurements of single-crystal olivine, even at room temperature, and we found it necessary to suppress radiative transfer at room temperature through use of graphite and sometimes metal coatings for the olivines measured here and previously analyzed garnets (Hofmeister 2006). Radiative transfer likely affects most previous thermal transport measurements of minerals. The above form does *not* describe the thermal diffusivity of garnets in experiments when radiative transfer was eliminated (Hofmeister 2006).

In summary, tradeoffs in fitting and the approximations needed to model the variable amounts of radiative transfer that are present in conventional and previous transient experiments on olivine make it difficult to ascertain their accuracy. The stated uncertainty of 5% (Gibert et al. 2005) apparently rests on calibration of Höfer and Schilling's (2002) results against previous measurements of quartz obtained using conventional methods (e.g., Kanamori et al. 1968; Beck et al. 1978), which *include* radiative transfer effects. Conventional measurements involving contact between heater, sample, and thermocouple can be uncertain by ~20%, as deduced by inter-laboratory comparisons (Ross et al. 1984). Hofmeister (2006) found that contact measurements on garnets at room temperature have uncertainties of 14%. Work in progress in our laboratory further shows that D_{lat} of any given quartz sample depends on its impurity content, including hydroxyl (Branlund and Hofmeister 2004). This observation is corroborated by measurements of garnets (Hofmeister 2006), the present work on olivine, and by the longstanding knowledge that impurity ions reduce D (e.g., Slack 1964). Hence we do not consider quartz to be a reliable standard on which to base calibrations. The unfortunate conclusion is that methods commonly used in geologic science fall short of providing accurate and independent measurements of phonon transport.

The goal of the present study is to address the above-mentioned issues for materials with the olivine structure. Specifically, accurate (~2% uncertainty) measurements of heat transfer by phonons are provided by using the laser-flash technique, which isolates *phonon* from *photon* transfer, as described briefly in the next section. To ascertain the dependence of thermal diffusivity on crystal chemistry for olivine-group minerals, we obtained a wide variety of natural and synthetic specimens and measured polycrystalline samples in addition to gem-quality single crystals (Table 1) and characterized our samples by IR spectroscopy and electron microprobe analysis.

BACKGROUND

The laser-flash technique

The laser-flash technique dates back to Parker et al. (1961) and is commonly used in material sciences; it was first used for geological problems by Buettner et al. (1998). Thin sample slabs are heated with a laser pulse from below while emissions of heat from the top of the sample is monitored with an IR detector (Fig. 1). The sample is not in direct contact with thermocouples, and neither is the differential heating supplied via contact, which circumvents the need to quantify power input and the possibility of (unknown) contact losses of heat.

The phonon component is separated from unwanted direct radiative transfer by use of either metal (Degiovanni et al. 1994) and graphite sample coatings and/or mathematical models (Mehling et al. 1998), as illustrated in Figure 1. The bottom graphite coating of ~1 μm thickness prevents laser light from reaching the sensitive IR detector and also serves as a basal heater by absorbing the energy of the laser pulse. Because the change in temperature across the sample associated with the pulse is small (≤4 K), the temperature dependence of D is determined solely by varying furnace temperature. As the heat diffuses by phonon collisions from the bottom coat up through the sample to the top coat, the temperature of the top coat gradually rises and thus emits more light, which is recorded by the IR detector in terms of signal voltage as a function of time (Fig. 1b). The top coat reaches a peak emission at some finite time after the laser pulse because phonons travel at roughly sound speeds.

TABLE 1. Description and composition of olivine thermal diffusivity samples

		Sample description	Comments/source
		Single crystals	
Fo [001]	Mg_2SiO_4	colorless, no fractures	synthetic, donated by R. Boehler
FoCo [010]	$Mg_{1.99}Co_{0.01}SiO_4$	pale blue, no fractures	synthetic, Morion Company
FoCo [001]			
Needles [100]	$Mg_{1.84}Fe_{0.16}SiO_4$	light green, no fractures	Excalibur Mineral Company
Needles [010]	250 ppm H_2O		
Needles [001]			
Needles [001]*			
Sumput [010]	$Mg_{1.87}Fe_{0.13}SiO4$ 60 ppm H_2O	light green, no fractures, minor small inclusions	Excalibur Mineral Company
sinhalite [010]	$MgAlBO_4$, 2.1 wt% FeO	light brown, gem quality	Sri Lanka, eBay purchase
chrysoberyl [100]	$BeAl_2O_4$, 0.5 wt% Cr_2O_3	yellow-green, no fractures	synthetic, Morion Company
chrysoberyl [010]		strong pleochroism	
chrysoberyl [001]			
		Polycrystalline samples	
dunite 1	~$Mg_{1.8}Fe_{0.2}SiO_4$	>95% ol, rest opx and cpx	Jackson County, NC (WUC)
dunite 2	~$Mg_{1.8}Fe_{0.2}SiO_4$	>95% ol, rest opx and cpx	Jackson County, NC (WUC)
Mn_2GeO_4	Mn_2GeO_4		synthetic, T. Young (UC Davis)
monticellite-bearing rock	$Ca_{1.15}Mg_{0.79}Mn_{0.06}SiO_4$	60% monticellite 40% epidote (?)	Excalibur Mineral Company
hortonolite-bearing rock	$Mg_{1.2}Fe_{0.8}SiO_4$	50% hortonolite 50% ilmenite	Harvard Collection, C. Francis
fayalite-bearing slag	~$Fe_{1.98}Mn_{0.02}SiO_4$	~85% Fa, <5% FeS, ~10% Pb-bearing flux	synthetic, Buffalo, NY (WUC)
fayalite-bearing rock	~$Fe_{1.84}Mn_{0.02}Mg_{0.14}SiO_4$	70% Fa, 15% Fe_2O_3/Fe_3O_4, ~15% Ca, Fe-rich silicate	Forsythe Mine, Quebec, Canada (WUC)

Notes: Fo is forsterite and FoCo is Co-doped forsterite. The Needles and Sumput olivines developed small fractures after repeated heating and some inclusions in the Sumput olivine became more visible, but all other samples showed no discernable changes, even after repeated heating episodes. The synthetic Fo [001] was grown after the method of Shankland and Hemmenway (1965), sample courtesy of R. Boehler. Mn_2GeO_4 prepared from regent grade oxides and hot-pressed to reduce pore space. WUC denotes samples from the Washington University mineral and rock collection.

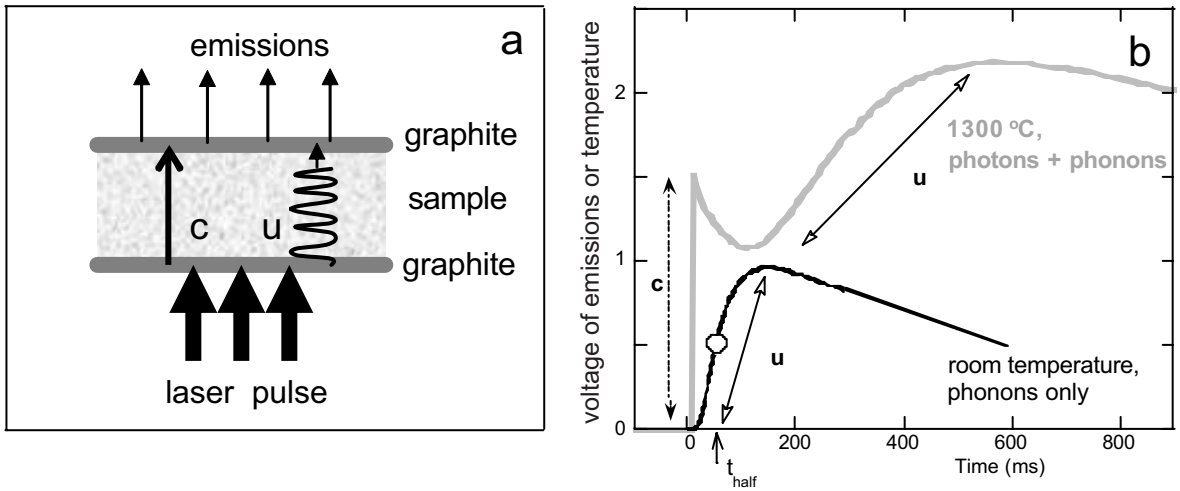

FIGURE 1. Principles of operation of a laser flash apparatus. (**a**) Physical transfer of heat during the experiment. A plate-shaped sample (stipple) is coated top and bottom with graphite and held at some given temperature in a furnace. Emissions (light arrows) from the top coat are recorded by an infrared detector, giving a baseline. The laser pulse (heavy arrow) is totally absorbed by the bottom graphite coat. Heat from the bottom coat then either traverses the sample as photons (medium arrow) near the speed of light (~c), or as phonons (squiggle arrow) at roughly the speed of sound (~u). For light-colored samples, essentially no absorption occurs and all radiative transfer is the boundary-to-boundary type shown here. (**b**) Corresponding record of heat transfer. Emissions are measured as signal voltage and set to zero before the laser pulse at $t = 0$. Model curves from our experiments are shown. At low temperature (black curve), emissions are low and radiative transfer is negligible. Virtually all heat is carried by the phonons, causing the emissions from the top coat to rise gradually with time since phonons travel near sound speeds. The position for the half rise time used in analysis (Eq. 1) is shown by the circle. The result is that the peak in emissions (temperature) of the top graphite coat lags behind the laser pulse. At high temperature, radiative transfer from the bottom coat warms the top coat, giving the sharp rise in emissions almost instantaneously (schematically shown at the dotted double arrow marked "c." The slower phonon travel occurs afterward, indicated by the solid double arrow marked "u." Emissions then decrease as the sample re-equilibrates with its surroundings.

Because emissions are directly related to temperature, the detector response is known as a temperature-time curve. Radiative transfer is negligible at low temperature due to the weakness of the emissions (i.e., this component is within the noise level of the detector). As temperature rises, radiative transfer between the graphite layers increases, and is recorded as a virtually in-

stantaneous rise in emissions immediately after the pulse (Fig. 1b) because photons travel at nearly the speed of light within a solid. Phonon and photon heat transfer contributions are thus visually discernable in the temperature-time curves (Fig. 1b) and are extracted using the mathematical model of Mehling et al. (1998). Their equations allow for absorbance being frequency dependent, although the detailed values of optical properties are not needed. Blumm et al. (1997) established model accuracy by comparing coated and uncoated samples. For further discussion of the method and background, see Hofmeister (2006).

Experimental uncertainty in laser-flash measurements is discerned from the simplest case of adiabatic heating with no radiative effects:

$$D = 0.1388\ L^2/t_{\text{half}} \quad (1)$$

where L is the thickness of the sample and t_{half} is half of the time required for temperature to reach the maximum after the laser pulse (Parker et al. 1961). Although this basic expression has been refined to allow for effects such as radiative heat loss from the front and back surfaces of the sample (Cowen 1963), D remains essentially proportional to the sample thickness and inversely proportional to time. Ambiguity in sample thickness is the main source of uncertainty, whereas time is measured with great accuracy. The accuracy for the technique is considered to be 2%, determined through benchmarking against opaque and soft standard reference materials (SRMs, obtained from the National Institute of Standards, NIST) such as metals and graphite (Blumm and Opfermann 2002), which have been accurately measured using conventional measurements.

The damped harmonic oscillator-phonon gas model for thermal diffusivity

Debye's (1914) analogy of the scattering of phonons to collisions of molecules in a gas forms the basis of all models of heat transport in insulators. Average properties of the phonons suffice because k and D are bulk physical properties, leading to

$$D(T) = \frac{< u(T) >^2}{6\pi Z < \text{FWHM}(T) >} = \frac{< u(T) >< \lambda(T) >}{3Z} \quad (2)$$

where Z is the number of formula units in the primitive unit cell, u is a velocity appropriate for the average phonon, FWHM is the Full Width at Half Maximum of peaks in the dielectric function, and λ is the mean free path of the phonons (Hofmeister 1999, 2001, 2004, 2006; Giesting and Hofmeister 2002).

Forms for temperature dependence of D are suggested by spectroscopic and elastic measurements. For forsterite and olivine, $\partial(\ln u)/\partial T$ is –0.006 to –0.008 %/K (Anderson and Isaak 1995). Raman spectra show that forsterite and olivine peak widths increase strongly with T (Kolesov and Geiger 2004a), values of $\partial(\ln \text{FWHM})/\partial T$ are near 0.14 %/K for three Raman peaks examined in detail, and that FWHM is finite near 5 K for Raman bands of fayalite (Kolesov and Geiger 2004b), leading to:

$$\frac{1}{D} = \frac{6\pi Z}{u_0^2}(FWHM_0 + aT + ...)(1 + bT + ...) \approx A + BT + CT^2 + ... \quad (3)$$

where a, A, etc., are constants. The linear coefficient B should dominate and has a positive sign. However, given that u does weakly depend on temperature, thermal diffusivity can also be represented by:

$$D \approx A + \frac{B}{T} + \frac{C}{T^2} + ... \quad (4)$$

Hofmeister (2006) found that $D(T)$ of garnets could be fit with either Equation 3 or 4, but that Equation 3 provided better fits.

At very high temperature, peak widths can become constant, resulting in constant values for D. In the kinetic theory of gases, mean free paths are connected with number of molecules per unit volume (e.g., Reif 1965). As temperature increases, overtone-combination modes are excited, but saturation in the number of modes occurs when T is high enough that the continuum dominates the statistics (see Mitra 1969). For silicate spinels, overtone-combinations are not observed above about ~2400 cm^{-1} (Hofmeister and Mao 2001), indicating that continuum statistics should control vibrational behavior at the energy equivalent temperature of ~1600 K, which is double the Debye temperature.

Experimental methods

Sample preparation

Oriented samples were prepared from mineral specimens with well-developed crystal faces. The correctness of the orientations was verified with a petrographic microscope and where necessary orientations were identified by IR spectroscopy (see below). All samples, including the non-oriented polycrystalline synthetic and natural samples, were initially cut as ~2–3 mm thick plates. Thinning and polishing produced samples with final thicknesses of 0.7–1.5 mm and parallel surfaces normal to the crystallographic axes. After conducting IR spectroscopic and electron microprobe measurements, samples were sand-blasted with alumina grit of 50–150 μm to rough up the surface for improved adhesion of metal and graphite coatings. In practice, such thin plates can become very fragile. To reduce extended sample handling and thus potential breakage of the samples, we accepted a variation of ±0.005 mm across the 6–10 mm diameter circular area to be analyzed; samples measured approximately 7–12 mm across. As the average thickness is well constrained, departures from parallelism, as well as surface roughness, do not contributed additional errors to D beyond the ~2% uncertainty established through comparison with standards, see below.

To enhance absorption of energy from the IR laser pulse by the samples and to shield the detector from laser light, top and bottom surfaces of the samples were coated either with Pt and then graphite or just with graphite. The graphite was applied as 3–5 thin layers on each surface while making sure that the previous layers were dry before application of subsequent layers. Total coating thicknesses of ~1 μm negligibly effect measurements of D from approximately millimeter-sized samples. Commercially available dry graphite spray was used and we found no significant differences between several brands.

Major-element sample characterization

All samples were characterized chemically by wavelength dispersive analysis (WDS) using standard procedures on the JEOL-733 electron microprobe at Washington University. The compositions of several samples were also verified by energy dispersive analysis using the JEOL JSM 840 SEM housed at the Department of Geology of the University of Illinois at Urbana-Champaign. Sinhalite and chrysoberyl contain light elements (B, Be) that cannot be detected by electron microprobe techniques. Instead, B_2O_3 and BeO were specified at constant ideal concentrations to be included in the ZAF corrections of the WDS analyses. We find that our sinhalite sample contains ~2.1 wt% FeO (all Fe as Fe^{2+}) and the Cr-doped chrysoberyl has ~0.5 wt% Cr_2O_3. Neither sample contains any other detectable minor elements. Compositions are given in Table 1.

Spectroscopic characterization of transition metal ions and hydroxyl

Near-infrared (IR) spectra were obtained at ambient conditions using an evacuated Bomem DA3.02 Fourier transform interferometer with an SiC globar source, a liquid N_2 cooled InSb detector, and a CaF_2 beamsplitter. About 2000 scans were collected from ~1800–8000 cm^{-1} using at a resolution of 2 cm^{-1} and the instrumental

accuracy is 0.01 cm^{-1}. Substituting a quartz lamp and beamsplitter provided the range ~3500–13000 cm^{-1}. A Si-avalanche detector was used at the resolution of 4 cm^{-1} to access the range ~9000 to 22000 cm^{-1}. For forsterite, polarized spectra were collected using a KRS5 wire grid polarizer. Segments were merged by shifting the more absorbent spectral segment downward by a constant so that the region of overlap matched, based on the assumption that surface imperfections cause scattering in some wavelength regions.

The spectral range of our instrument allows measurement of the overtones of the lattice vibrations, O-H stretching modes, and the d-d electronic transitions of various species found in our samples: Fe^{2+}, Co^{2+}, and Cr^{3+}. However, the spectrometer does not reach high enough frequencies to probe bands due to Fe^{3+}. Absorbance was calculated using the convention:

$$a = -\log(I_{trans}/I_0). \quad (5)$$

The corresponding absorption coefficient, A, equals a/t where t is thickness. Precise values of OH^- content require a calibration based on sample chemistry. For forsteritic olivine, hydroxyl contents were calculated from:

$$H_2O \text{ (in ppm by weight)} = 0.188 \text{ IA} \quad (6)$$

where $IA = \int a(\nu)d\nu/t$ is the integrated absorbance from ~3450 to 3730 cm^{-1} (Bell et al. 2003). Unfortunately, intensity calibrations are not available for Cr^{3+} or Co^{2+}.

The spectra in Figure 2 are from samples used to measure D and indicate that optically thin conditions exist in the near-IR, which is the locus of the blackbody peak at the temperatures of our experiments. The peak position is governed by Wein's law: ν_{max} (in cm^{-1}) = 3.451T (K).

Sinhalite

The natural sinhalite sample has weak, sharp bands at 3478 and 3508 cm^{-1} and a broad band at 3302 cm^{-1} (Fig. 2a) that were observed previously and attributed to O-H stretching (Bauerhansl and Beran 1997). Our cut gemstone has additional OH bands at 3545 and 3649 cm^{-1}, but not the 3474 cm^{-1} band observed by Bauerhansl and Beran (1997); these differences could be due to sample chemistry. Because intensities are low, the amount of water is low as well. The amount was not quantified as the sample was not large enough to gather spectra from all three orientations. The broad peak at 9179 cm^{-1} and the shoulder at 8737 cm^{-1} are due to electronic transitions of Fe^{2+}. These peak positions agree with the study of Farrell and Newnham (1965). Based on the polarized spectra of Bauerhansl and Beran (1997) and Farrell and Newnham (1965), the presence of the 3302 and 8737 cm^{-1} bands, and the absence of a band at 10810 cm^{-1} indicates that the sinhalite orientation is [010].

As a rough approximation, we assume that the intensity of Fe^{2+} bands in olivine is the same as that of sinhalite. Direct comparison (Fig. 2a) suggests that our sample has 0.042–0.048 cations Fe^{2+} per formula unit (pfu), in reasonably good agreement with the ~2.1 wt% FeO or 0.036 cations of Fe^{2+} pfu as determined by electron microprobe analysis.

Chrysoberyl

The synthetic chrysoberyl samples lack OH absorptions and absorptions attributable to Cr^{3+} occur above 8000 cm^{-1}. Our peak positions do not exactly match those in the polarized measurements of Farrell and Newnham (1965), but their polarization information allowed us to confirm the orientations of the three slabs

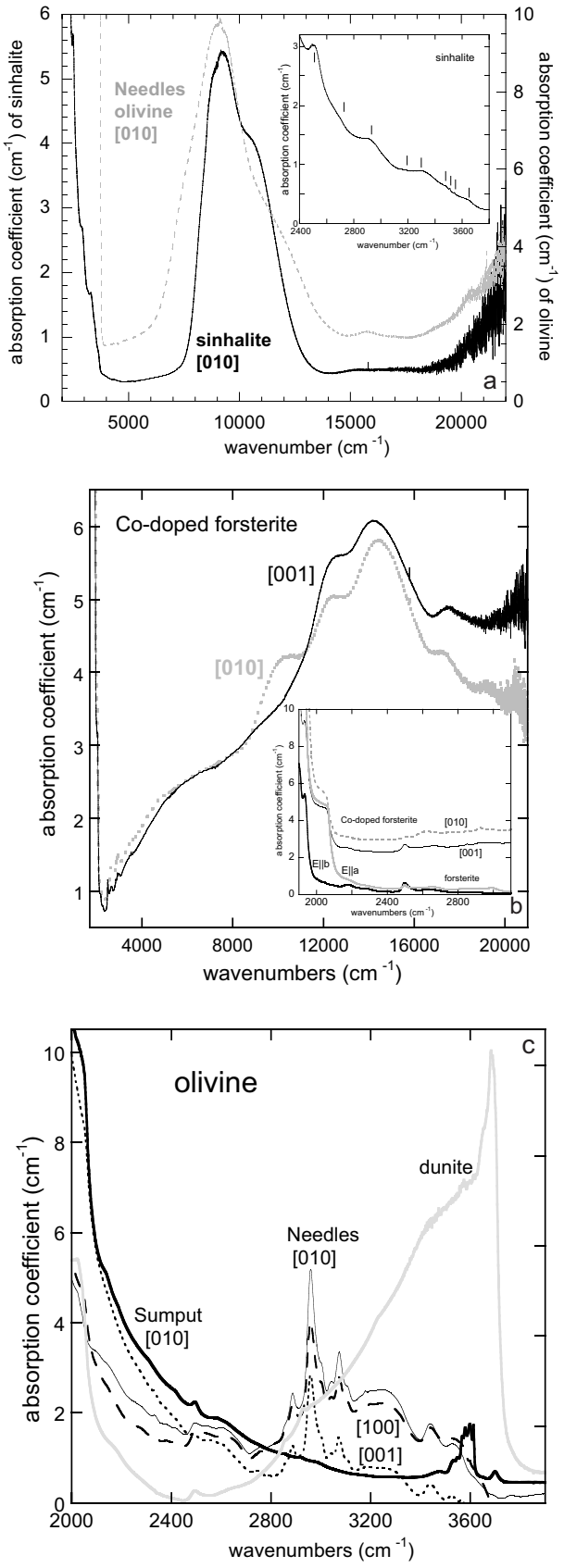

FIGURE 2. Absorption spectra of olivine analogs. (**a**) Sinhalite with comparison to olivine: the intense band at 900 cm^{-1} is due to Fe^{2+} in sinhalite (black curve). The same orientation of olivine is shown as the gray dotted curve. Inset shows the O-H bands and overtones of sinhalite. Tick marks indicate peak positions. (**b**) Co-doped forsterite and forsterite: solid curve = [001], dotted curve = [010]. All broad bands are due to Co^{2+} transitions. Inset: comparison of overtone spectra with forsterite; heavy solid curve = **E**||**b** of forsterite; gray curve = **E**||**a** of forsterite; light solid curve = [001] of Co-doped sample; dots = [010] of Co-doped sample. (**c**) Absorption spectra of the overtone and O-H stretching spectral regions for various forsteritic olivines. Gray curve = dunite; heavy solid curve = [010] of Sumput olivine; light curves are the three faces of Needles olivine.

cut from our sample of synthetic chrysoberyl. Peak positions measured here are in good agreement with those of Scalvi et al. (2003), and a few additional weak, narrow bands are resolved. Narrow bands (R lines) exist at 14696, 14734, 15066, 15275, 15434, 15510 cm^{-1}, and broad bands occur at ~9385, 17050, and >22000 cm^{-1}. An intensity calibration is unavailable, and thus Cr^{3+} contents cannot be ascertained from our spectra. However, electron microprobe analysis shows the presence of ~0.5 wt% Cr_2O_3, matching the manufacturer's specifications for this sample.

Co-doped forsterite

Synthetic, Co-doped forsterite has no detectable O-H absorptions: peaks between 1800 and 3200 cm^{-1} (Fig. 2b, inset) are attributed to overtone-combination bands. Comparison to spectra of synthetic forsterite was used to determine the orientations. Absorptions attributable to Co^{2+} occur in [001] at 5650, 12300, 14200, 17530, and ~20000 cm^{-1} and in [010] at 4850, 10046, 12300, 14400, 17300, 19200, and ~20000 cm^{-1} (Fig. 2b). Peak positions are approximate because the spectra were not deconvoluted. The bands at 5650 and 4850 cm^{-1} are very weak and broad and seem to be artifacts of scattering combined with spectral merging. Spectroscopic measurements were previously made only of olivines with high concentrations of cobalt: Co_2SiO_4, $Co_{1.28}Mg_{0.72}SiO_4$, $Co_{0.25}Mg_{1.75}SiO_4$, (Taran and Rossman 2001; Ullrich et al. 2004). Observation of six bands is consistent with partitioning of Co into the distorted M1 site (e.g., Miyake et al. 1987) and with the assignments of Taran and Rossman (2001). Our spectral pattern is consistent with these previous studies, and the polarizations are similar, but peak positions differ significantly from those of high Co samples. The six positions for Co in M1 are 8300, 8650, 13300, 16000, 19500, and 21000 cm^{-1} (Taran and Rossman 2001) which are ~0 to 3650 cm^{-1} lower than ours. Ullrich et al. (2004) assign the 13300 cm^{-1} band to M2, whereas both sites are assigned to this band by Taran and Rossman (2001). The cation sites for our sample with low concentrations of Co should be equal to those of forsterite, whereas the high Co samples have significantly expanded M1 and M2 sites (Miyake et al. 1987). The high frequencies in our study are attributed to stuffing Co into the small, unexpanded Mg-site.

H_2O in mantle olivine

The O-H spectral region differs significantly among our natural olivine samples from three different localities (Fig. 2c). Peaks in the Needles specimen near 2800–3000 cm^{-1} are C-H stretches probably due to residual acetone and were not included in calculating the hydroxyl content (250 ± 50 ppm H_2O by weight). The spectral signature of Needles samples closely resembles those of previously measured olivines (e.g., Bell et al. 2003). Sumput olivine has fairly weak hydroxyl peaks near 3600 cm^{-1}, corresponding to 60 ± 20 ppm H_2O by weight. Dunite has a broad band near 3400 cm^{-1}, consistent with molecular water, and a hydroxyl peak at 3650 cm^{-1}, consistent with the presence of an alteration product. All three Needles mantle olivine orientations have absorptions near 10000 cm^{-1}, attributable to d-d transitions of Fe^{2+}. The spectra are as previously observed (e.g., Burns 1970) and only the [010] orientation is shown here (Fig. 2a).

Laser-flash analysis and data processing

Thermal diffusivity was measured with a LFA 427 laser flash apparatus made by Netzsch Gerätebau, Germany. For a more detailed description of the LFA 427, see Bräuer et al. (1992) and Blumm and Lemarchand (2002). Depending on sample size, specimens were held in graphite holders that allow analysis of a circular area with a diameter of 6 or 10 mm. A single pulse from an Nd-GGG laser heated the sample from below; heat diffused from the bottom to the top of the sample, and emissions were monitored by an InSb detector mounted above the sample. The laser wavelength was 1064 nm and typical settings for the pulse were 325–340 V with widths of 0.5–0.8 ms. These laser pulses are of much shorter duration than heat diffusion across the samples. Data were acquired as time-temperature curves of ~10^2–10^4 ms in duration (Fig. 3). The sample was located in the hot-spot zone of a vertical furnace and the temperature dependence of thermal diffusivity was obtained by simply varying the furnace temperature. Temperature was measured and controlled by two W-Re thermocouples, one located adjacent to the sample, the other being inside the furnace. Room-temperature readings were confirmed with a calibrated thermometer. Thermocouple calibration and stability at elevated temperature were verified repeatedly over the 6-month period in which the measurements for this study were conducted. The Curie transitions of pure Fe (770 °C) and Co (1113 °C) metals were found to be at 787 °C and 1125–1130 °C, respectively, and the α-β transition of quartz (573 °C) was located at 588 °C. The temperatures reported in this study are corrected on this basis. Temperature gradients across the sample are presumed to be negligible because the gradient across the furnace chamber is low, <10 °C over ~100 mm. Data were acquired in an Ar gas atmosphere: before each analytical run, sample and furnace chambers were evacuated and flushed 2–3 times with high purity (5.0 or 6.0) grade Ar gas. Analyses were performed at a slight overpressure near 1.1 atmospheres, maintaining a constant Ar gas flow of ~100 mL/min. The inert gas serves two purposes: (1) It reduces the concentration of oxygen in the sample and furnace assembly. A controlled oxygen fugacity is necessary at high temperatures to avoid unwanted oxidation of Fe-bearing samples and extend the stability of Pt and graphite coatings on samples to higher temperatures. Sample holders and caps are manufactured from high-purity graphite and the presence of graphite thus buffers the oxygen fugacity at high temperatures to C-CO. None of our Fe-bearing olivine samples show signs of oxidation, even after repeated and extended heating they remain transparent and green. (2) The gas flow aids thermal equilibration of sample and sample holders, thus eliminating unwanted effects from potentially small temperature gradients across samples and/or sample holders located in the hot zone of the furnace assembly.

Thermal diffusivity values at temperature were verified against electrolytic iron (SRM-8421). Applying Cowan's (1963) model to our measurements reproduces D overall from 298 to 1073 K on this specific material obtained using another laser flash apparatus (Monaghan and Quested 2001). Specifically, values agree to ~5% near the Curie transition of Fe and ≤2% at T well below and above the transition, supporting the notion that accuracy of the laser-flash method is better than conventional methods, as discussed earlier. Good agreement was also obtained with NIST data on austenitic stainless steel (SRM-1460) (Henderson et al. 1998) and with inter-laboratory comparisons of graphite (Blumm and Lemarchand 2002).

In a typical analytical run, data were obtained at 50–100 °C intervals with three acquisitions at each temperature. Data acquisition was ended when D values no longer changed significantly or when data quality declined. The latter was caused by physical separation of the graphite coating from both top and bottom of the sample slabs, resulting in significantly increased radiative heat transfer and irregular signal curves. When coatings did not deteriorate at high temperature and no other changes such as phase transitions or melting occurred in samples, data measured during cooling of an analytical cycle were in excellent agreement with data collected during heating.

Data were processed with software provided by Netzsch. The inputs are sample thickness L and temperature-time curve. Raw data were automatically corrected for baseline drift of the InSb detector. The resulting data were evaluated carefully: data with erratic signal curves or overly large radiative components and apparent discrepancies between model fits and measured data were discarded. We use the algorithm of Mehling et al. (1998) to model thermal diffusivity and take into account radiative surface losses, as well as corrections for the measured shape of the laser pulse (Blumm and Opfermann 2002). Examples are given in Figure 3, showing typical data signals acquired at three different temperatures from a single olivine sample: at room temperature no radiative heat transfer was observed (Fig. 3a). Only above ~700–800 °C does radiative heat transfer become significant for olivines (Fig. 3c).

Results

For all samples, thermal diffusivity is highest at room temperature, and then decreases with rising temperature until D becomes virtually independent of temperature at high temperatures (Figs. 4–10). Table 2 lists room temperature diffusivity, the values at the highest measured temperature, and D values at 150–200 °C *below* the highest measured temperature. The latter information serves to illustrate that thermal diffusivity indeed becomes significantly less dependent on temperature at high temperatures.

Needles olivine exhibits room temperature D values of 3.25, 1.66, and 2.59 mm^2/s for [100], [010], and [001], respectively (Fig. 4). These values decrease to 0.93–0.87 mm^2/s at 790–985 °C for [100], 0.54–0.51 mm^2/s at 590–740 °C for [010], and 0.83–0.79 mm^2/s at 740–890 °C for [001]. The Needles [001]* sample has a room temperature diffusivity of 2.7 mm^2/s, decreasing to a virtually constant value of 0.79 mm^2/s at 1180–1380 °C (Fig. 5). The Sumput olivine [010] orientation has a thermal diffusivity close to that of Needles [010], namely 1.59 mm^2/s at room temperature and 0.56 mm^2/s near 590 °C (Fig. 4).

Room-temperature thermal diffusivity is 5.15 mm^2/s for

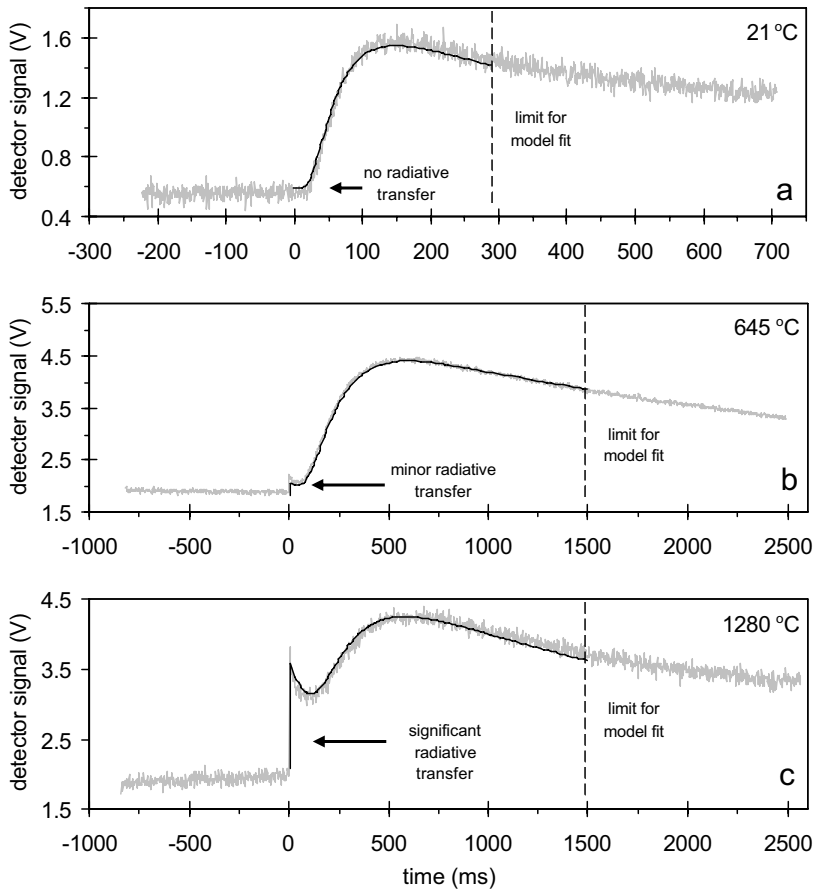

FIGURE 3. LFA signals acquired at various temperatures and varying radiative transfer component. The three detector signals and model fits of the [001] orientation of Co-doped forsterite at (**a**) 21, (**b**) 645, and (**c**) 1280 °C. Note the absence of detectable radiative transfer at room temperature; at high temperature (**c**) the mis-fit between data (light curve) and Mehling's (1998) model (dark line) become noticeable, indicating that very-high temperature data have larger uncertainties.

TABLE 2. Thermal diffusivity values of olivine

	Room temperature			High temperature			Max. temperature		
Sample	*T* (°C)	*D* (mm²/s)	*n*	*T* (°C)	*D* (mm²/s)	*n*	*T* (°C)	*D* (mm²/s)	*n*
Fo [001]	18(1)	5.14(4)	5	790(4)	1.13(1)	2	985(3)	0.98(1)	3
FoCo [001]	21(2)	4.17(11)	6	1280(1)	0.72(1)	2	1477(1)	0.65(1)	2
FoCo [010]	19(3)	2.60(14)	4	986(1)	0.44(2)	3	1181(1)	0.40(1)	2
Needles [100]	20(1)	3.25(12)	7	788(2)	0.93(1)	3	985(2)	0.87(1)	3
Needles [010]	21(2)	1.66(4)	6	591(1)	0.54(1)	3	739(1)	0.51(1)	2
Needles [001]	20(1)	2.60(3)	6	738(1)	0.83(1)	3	886(1)	0.79(1)	3
Needles [001]*	18(1)	2.69(7)	8	1184(1)	0.79(3)	4	1379(1)	0.79(7)	6
Sumput [010]	20(1)	1.59(3)	6	588(1)	0.56(1)	6	983(1)	0.47(1)	3
sinhalite [010]	19(4)	5.30(22)	6	544(2)	1.05(1)	3	741(3)	0.82(2)	3
chrysoberyl [100]	21(1)	8.99(10)	5	817(1)	1.51(1)	3	990(2)	1.32(2)	3
chrysoberyl [010]	20(1)	6.22(12)	4	792(1)	1.10(3)	3	989(1)	0.92(3)	3
chrysoberyl [001]	20(1)	8.42(13)	5	816(1)	1.50(3)	3	990(2)	1.32(3)	3
dunite 1	19(1)	2.31(4)	12	692(2)	0.62(1)	3	888(3)	0.55(1)	3
dunite 2	20(2)	2.05(4)	11	888(3)	0.58(1)	3	1083(2)	0.56(1)	3
Mn_2GeO_4	18(3)	1.24(4)	4	497(7)	0.46(1)	3	699(1)	0.42(1)	3
monticellite-bearing rock	19(1)	1.17(1)	3	699(3)	0.56(1)	5	895(2)	0.54(1)	6
hortonolite-bearing rock	19(2)	1.47(2)	12	500(8)	0.67(1)	3	695(6)	0.61(1)	3
fayalite-bearing slag	20(2)	0.80(1)	6	692(3)	0.38(1)	3	886(1)	0.35(1)	3
fayalite-bearing rock	20(3)	1.27(2)	10	692(4)	0.47(1)	3	887(3)	0.43(1)	3

Notes: Samples with orientations indicate single crystals; other samples are polycrystalline. *n* indicates number of individual measurements used to obtain reported averages. Uncertainties in *T* and *D* should be read as follows: Fo[001] has $D = 5.14 \pm 0.04$ mm²/s at 18 ± 1 °C. Needles [001]* max. *T* data averaged from three measurements at indicated *T* and three interpolated data points derived from data taken at higher and lower temperatures; note the much larger uncertainty compared to FoCo[001] at similar *T*.

forsterite [001], which decreases to 0.98 mm²/s near 985 °C (Fig. 5). The Co-doped forsterite has slightly lower values for [001]; 4.17 mm²/s at room temperature and 0.72 to 0.65 mm²/s at 1280–1477 °C. The corresponding [010] orientation has values of 2.60 at room temperature and 0.44–0.40 mm²/s at 985–1180 °C, respectively.

For chrysoberyl, $D_{[100]}$, $D_{[010]}$, and $D_{[001]}$ at room temperature are 9.0, 6.2, and 8.4 mm²/s, respectively (see Figs. 6, 7, and 8). $D_{[100]}$ and $D_{[001]}$ become virtually identical with values of 1.5–1.3 mm²/s at 816–990 °C and the $D_{[010]}$-value is 1.1–0.9 at 790–990

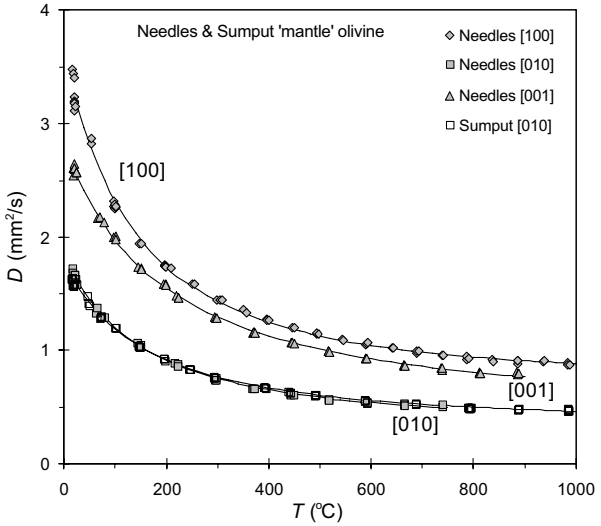

FIGURE 4. Thermal diffusivity of olivine single crystals as a function of temperature. Symbols mark the acquired data; all shown data were used to fit the curves (dark lines) with Equation 4; there is very good agreement between data and fits over the entire range of temperatures. The Needles and Sumput olivine compositions are similar to olivine in Earth's upper mantle. Note the significant decrease of D with increasing temperature for all three crystallographic orientations and the good agreement of the [010] orientation for the separate samples. Despite initially different D values at room temperature, D values become very similar at elevated temperature, regardless of crystallographic orientation.

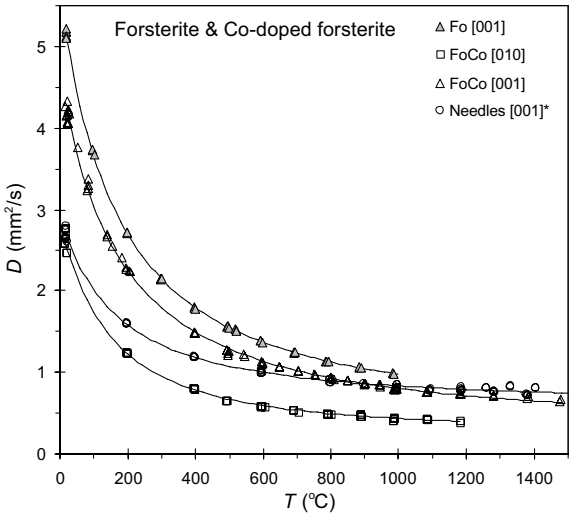

FIGURE 5. Thermal diffusivity of pure and Co-doped forsterite single crystals and Needles [001]*. The [001] orientation of the pure forsterite is expected to be the lowest D value of all three orientations for this sample, hinting at much higher thermal diffusivities for pure end-members when compared to extensive solid solutions. Small amounts of impurities, such as the 0.3 wt% CoO in the Co-doped olivine, seem to have little effect on thermal diffusivity as values for [001] of the pure and Co-doped samples are very similar at room and elevated temperatures. The [001] data of the Co-doped forsterite and Needles [001]* illustrate that D values become virtually independent of T at very high temperatures.

°C. The [010] orientation of sinhalite has a room-temperature D-value of 5.3 mm²/s, diminishing to 1.05–0.82 mm²/s at 540–740 °C (Fig. 7).

For the polycrystalline samples (Fig. 9), dunite 1 has a thermal diffusivity of 2.31 mm²/s at room temperature, compared to 2.06 mm²/s for dunite 2. These values decrease to 0.62–0.55 at 690–890 °C for dunite 1 and 0.58–0.56 mm²/s at 890–1080 °C for dunite 2. The two dunite specimens are from the same locality, but were cut from two separate hand samples; no deliberate attempt was made to obtain samples oriented in any particular direction. At room temperature, the structural analog Mn_2GeO_4 sample has D values of 1.24 mm²/s and D decreases to 0.46–0.42 at 500–700 °C (Fig. 9). Monticellite and hortonolite-bearing natural samples have room temperature thermal diffusivities of 1.17 and 1.47 mm²/s, respectively, decreasing to 0.56–0.54 mm²/s at 700–900 °C and 0.67–0.61 mm²/s at 500–700 °C, respectively (Fig. 9). The synthetic fayalite-bearing slag sample has diffusivity values of 0.80 and 0.38–0.35 mm²/s for room temperature and 690–890 °C, whereas the natural fayalite-bearing rock has corresponding values of 1.27 mm²/s and 0.47–0.43 mm²/s for the same temperature range (Fig. 10).

The resulting thermal diffusivity data were fitted against temperature, using the expression $D = a + b/T + c/T^2$ (Eq. 4), with the exception of the Mn_2GeO_4 sample, which required higher order (up to $1/T^4$) terms. The fitting coefficients for all samples are listed in Table 3. Fits used all the available data over the entire measured temperature range for each sample. Other expressions used to describe D as a function of temperature, such as $1/D = a + bT + cT^2$ (Eq. 3) or $D = D_0/(a + bT)$ proved less satisfactory.

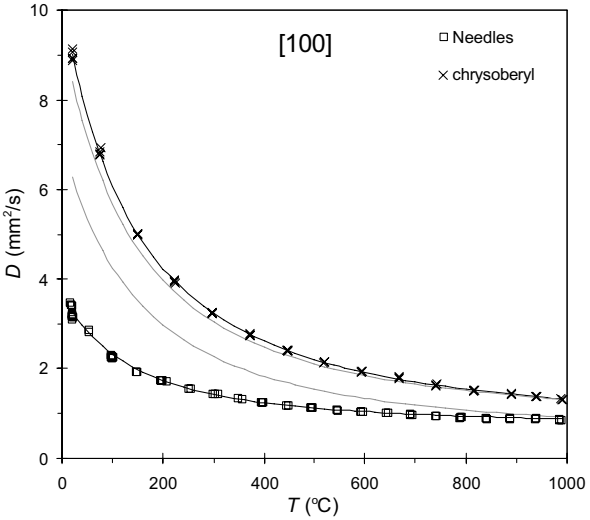

FIGURE 6. Comparison of the thermal diffusivity for the [100] directions of Needles olivine and chrysoberyl; the light lines indicate the remaining two orientations of chrysoberyl.

In some cases, the latter forms would have required separate fits for low and high temperatures, which we chose to avoid. For previously published measurements, due to the larger errors associated with conventional measurements, simpler forms for D were sufficient. However, the precision of our new data set warrants inclusion of the parameter c for [100] and [010], and it is absolutely necessary to include c for [001].

TABLE 3. Coefficients for fits of thermal diffusivity vs. 1/T (K)

Sample	Coefficients				
	a	b	c	R^2	max. T (°C)
Single crystals					
Fo [001]	0.3081	679.6	213492	0.9999	985
FoCo [001]	0.2347	587.8	172482	0.9986	1477
FoCo [010]	0.2415	115.4	165515	0.9967	1181
Needles [100]	0.7088	57.7	202533	0.9964	985
Needles [010]	0.3100	100.6	86470	0.9979	739
Needles [001]	0.3805	381.3	79703	0.9992	886
Needles[001]*	0.5701	248.43	108238	0.9974	1379
Sumput [010]	0.3135	127.2	73824	0.9987	983
sinhalite [010]	0.5546	−128.1	432571	0.9973	741
chrysoberyl [100]	0.5366	551.7	566872	0.9996	990
chrysoberyl [010]	0.3516	415.2	388978	0.9992	989
chrysoberyl [001]	0.6371	428.2	543382	0.9996	990
Polycrystalline samples					
dunite 1	0.2291	290.0	92938	0.9991	888
dunite 2	0.3563	178.4	93356	0.9988	1083
Mn_2GeO_4*	1.4099	−2520.3	2161696	0.9962	699
monticellite-bearing rock	0.3816	153.0	23706	0.9956	985
hortonolite-bearing rock	0.2826	301.2	12638	0.9979	705
fayalite-bearing slag	0.2637	83.9	21216	0.9990	886
fayalite-bearing rock	0.1798	265.3	15688	0.9993	887

Notes: Thermal diffusivity $D = a + b/T + c/T^2 ...$; T in K. R^2 indicates goodness of fit. Max. T: highest T included in fit; extrapolation beyond may be inaccurate if trend is not flat enough.
* Fit is 4th order polynomial with $d = -7.165 \cdot 10^8$ and $e = 8.622 \cdot 10^{10}$.

DISCUSSION

IR to visible spectra of our olivine samples lack intense bands like those in SmGG, which violate the optically thin conditions assumed in Mehling et al.'s (1998) model (Hofmeister 2006). Instead, our samples are either (1) optically thin and have moderately to weakly absorbing broad bands of transition metal ions or O-H bands that are narrow but very weak and at low frequency (Fig. 2), hence radiative transfer should be removed by the model, or (2) are opaque (Mn_2GeO_4, hortonolite and fayalite) and simply do not transmit radiatively within the temperature range investigated. The results (Figs. 4–10) support our contention that radiative transfer is completely removed in our experiments in that the opaque, Fe-rich rock samples have similar curves for $D(T)$ as both transparent (forsterite) and the partially transparent samples with various cations and spectral characteristics (Fig. 2). The olivine samples and olivine-rich rocks have $D(T)$ that decreases sub-parallel (Figs. 4–10) such that the range in D among the samples decreases with T. Similar behavior was seen for garnets (Hofmeister 2006) and attributed to a correlation of D at 298 K with dD/dT at 298 K and the dominance of the oxygen sub-lattice in controlling thermal diffusivity. Only the monticellite-bearing sample diverges from the trends, and this is attributable to the large proportion of secondary phases (~40%, Table 1). The sub-parallel trends for each of the olivines and garnets are clearly not a radiative transfer effect, given the diverse types of absorption spectra and intensity of absorptions present in the samples examined (22 garnets and 12 olivine group samples, all chemically distinct). We conclude that our measurements isolate the phonon component to the greatest extent so-far achieved in heat transfer studies of minerals, and most likely completely remove this unwanted component. Additional supporting evidence stems from the observation that $D(T)$ curves for both the olivines measured here and garnets (except SmGG) of Hofmeister (2006) approach a constant value at high temperature.

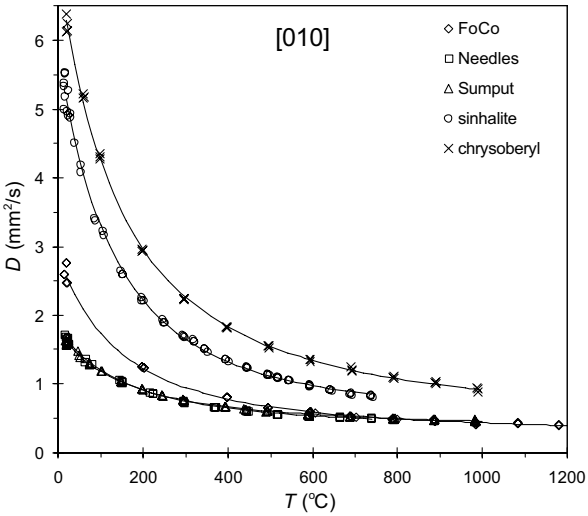

FIGURE 7. Thermal diffusivity of the [010] orientation for olivine-group single crystals. Agreement for $D_{[010]}$ of Needles and Sumput olivines is excellent. The Co-doped olivine (FoCo) has higher values at lower temperatures before data converge with the Needles and Sumput samples at 600–1000 °C. Sinhalite ($MgAlBO_4$) and chrysoberyl ($BeAl_2O_4$) have by far the highest thermal diffusivity.

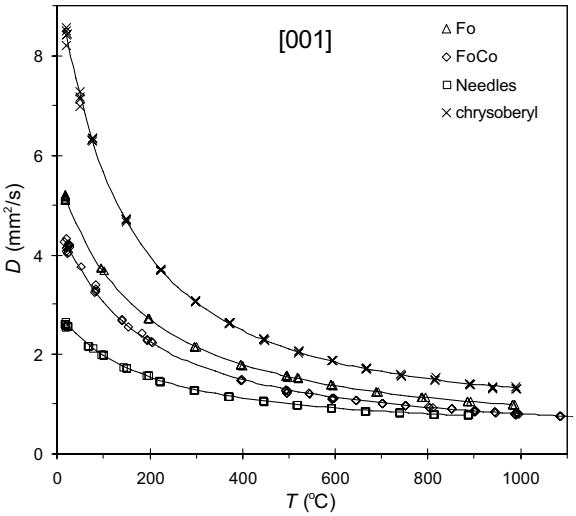

FIGURE 8. Thermal diffusivity of the [001] orientation for olivine-group single crystals. Chrysoberyl ($BeAl_2O_4$) has the highest observed D, forsterite and Co-doped forsterite have intermediate values, and Needles olivine has the lowest thermal diffusivity. Again, despite the initially varying room-temperature D values, the thermal diffusivities become similar at elevated temperatures.

Both types of radiative transport are strongly temperature dependent (Clark 1957; Shankland et al. 1979; Hofmeister 2005) and such effects on previous experimental measurements increase non-linearly with temperature. As discussed in the introduction, formulations for diffusive radiative transport are not relevant to laboratory experiments because frequencies exist where the light crosses the sample essentially unattenuated (Fig. 2 at ~4000 cm^{-1}), and thus the optically thick conditions

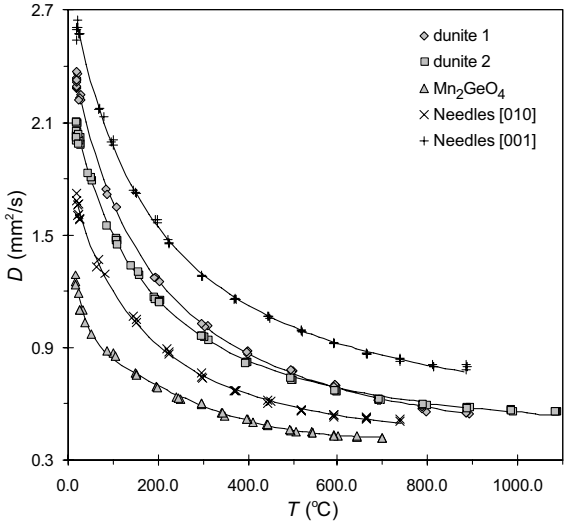

FIGURE 9. Thermal diffusivity of polycrystalline samples compared with selected oriented single crystal data. Dunites 1 and 2 have slightly different D values at room temperature, intermediate to [010] and [001] of the Needles single crystal of similar composition. The dunite 1 and 2 samples were cut at random orientations from separate hand specimens but have very similar D at high temperature. This indicates that bulk thermal diffusivity is defined by individual small crystals that exhibit a preferred orientation of [010] and [001] with no or negligible [100] or, alternatively, is dominated by [010] oriented grains with variable contributions from [001] and/or [100].

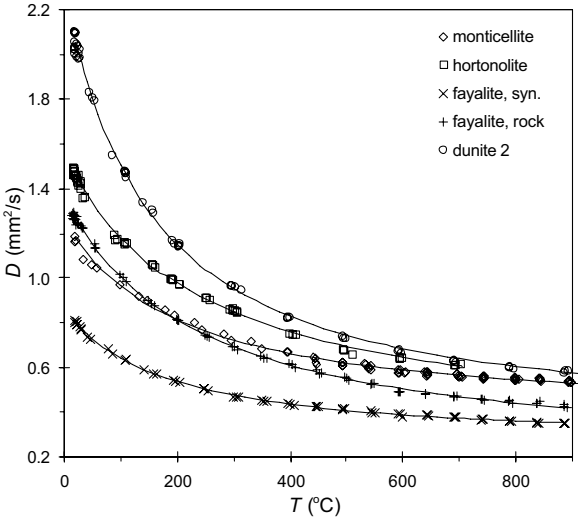

FIGURE 10. Thermal diffusivity of polycrystalline samples that contain monticellite, hortonolite, and fayalite. This figure illustrates the overall effect of olivine composition on thermal diffusivity of aggregate samples. Despite varying olivine contributions, overall D values are low for various samples; unfortunately, this does not rule out contributions from other minerals or phases present. For example, the synthetic fayalite-bearing slag sample contains a Pb-bearing flux that quenched to a glass. This results in the overall lowest observed thermal diffusivity of all samples because glasses tend to have much lower thermal diffusivity than minerals (see text).

needed for diffusive transfer are violated. Consequently, previous measurements of D at temperature consist of unknown proportions of phonon and photon transport. The disagreements that exist between our results for the phonon component of $D(T)$ and those inferred in previous studies (e.g., Kanamori et al. 1968; Gibert et al. 2003a, 2005) are therefore not examined in detail. Contact losses to thermocouples in these earlier studies may also contribute uncertainties in temperature derivatives of D, which can be systematic, as discussed in previous work.

Room-temperature D values for mantle olivine

The anisotropy of thermal diffusivity in olivine is well known (e.g., Kobayashi 1974; Chai et al. 1996; Gibert et al. 2003a, 2005). The compositions of our Needles and Sumput samples are close to those used by other workers and representative of olivine typically found in Earth's upper mantle (near Fo_{90}). In agreement with the above studies, we find that the order of D values for the different orientations at room temperature is $D_{[100]} > D_{[001]} > D_{[010]}$ (Tables 2 and 4). The values published by Kobayashi (1974) and Chai et al. (1996) coincide remarkably well, but newer thermal diffusivity data by Gibert et al. (2003a, 2005) are noticeably higher for all three orientations (Table 4); the values cited by Oasako et al. (2004) are intermediate for all three orientations. Our new data agree with Gibert et al.'s findings for $D_{[010]}$ and $D_{[001]}$, but our value for $D_{[100]}$ is much higher (3.3 vs. their 2.7 mm²/s, Table 4). Our two olivine specimens appear slightly more magnesian than the sample used by Gibert et al. (2003a, 2005), but the total range is Fo_{90}-Fo_{93} for all samples and we believe that this compositional difference is negligible. We verified the accuracy of the orientations of our samples with a petrographic microscope: the [010] and [001] orientations are correct, but there is a <10° misorientation for [100]. The Needles [001]* sample is also slightly misoriented and contains a small (~5–10°) component of the [100] orientation, which results in slightly elevated room temperature D values compared to the pure [001] sample (Tables 2 and 4); this sample was used obtain data at temperatures of up to 1400 °C (Table 2). Because the [100] orientation has the highest D values of any orientation, any misalignment would only lower this value—thus making our measured value of 3.3 mm²/s for $D_{[100]}$ a minimum estimate. Our technique thus provides a much higher value for $D_{[100]}$ compared to Gibert et al. (2003a).

In this context, it is useful to examine the ratios of thermal diffusivities for the different orientations: at room temperature, $D_{[100]}/D_{[010]}$, $D_{[100]}/D_{[001]}$, and $D_{[010]}/D_{[001]}$ determined in this study agree very well with those of Kobayashi (1974), despite the difference in absolute values (Table 4). There is also agreement in $D_{[010]}/D_{[001]}$ for Chai et al. (1996) and Gibert et al. (2003a) and Osako et al. (2004), though the data for $D_{[100]}/D_{[010]}$ and especially $D_{[100]}/D_{[001]}$ of Gibert et al. (2003a, 2005) differ most from published data and our new results. Gibert et al. (2003a, 2005) use the thickest sample for their [100] measurements (their sample 5, 9.1 mm thickness) and claim to already encounter significant radiative heat transfer at room temperature—in contrast, we do not observe radiative heat transfer at room temperature in our laser-flash measurements (Fig. 3a). This discrepancy may result from over-correcting (and hence lowering) of D values by Gibert et al. (2003a, 2005) and/or stem from a combination of different factors, including sample heating methods. As previously mentioned, our laser pulse is significantly shorter in duration when

TABLE 4. Comparison with thermal diffusivity data from the literature

D	This study	Kobayashi	Chai et al.	Osako et al.	Gibert et al.
[100]	3.25(12)	2.18	2.16	2.5	2.73(4)
[010]	1.66(4)	1.07	1.25	1.5	1.70(12)
[001]	2.59(3)	1.71	1.87	2.2	2.49(14)
D-ratios					
[100]/[010]	1.96	2.04	1.73	1.67	1.61
[100]/[001]	1.25	1.27	1.16	1.14	1.10
[010]/[001]	0.64	0.63	0.67	0.68	0.68
Composition	Fo_{92}	Fo_{92}	Fo_{89}	Fo_{93}	Fo_{91}
Method	LFA	mod. angstrom	PTGS	Angstrom	FHTM

Notes: All data at room temperature. Methods as follows: LFA = Laser Flash Analysis; mod. angstrom = modified angstrom method; PTGS = Picosecond Transient Grating Spectroscopy; FHTM = Filament Heating and Thermocouple Method. Complete references are Kobayashi (1974), Chai et al. (1996), Osako et al. (2004), and Gibert et al. (2003a, 2005).

compared to the overall length of acquired signal (<1 ms pulse vs. 500–1000 ms for heat transfer across the sample); additionally, our sample coatings suppress radiative heat transfer at room temperature. The heat pulse used by Gibert et al. (2003a) was much longer in duration, presumably 5–10 seconds, according to the method as described by Höfer and Schilling (2002), and data were collected for ~45 seconds. Gibert et al. (2003a) also use the T^3-law for processing the radiative contribution, shown by Shankland et al. (1979) to not be well suited for olivine. Nevertheless, despite the disagreement for $D_{[100]}$, there is good agreement of $D_{[010]}$ and $D_{[001]}$ between Gibert et al. (2003a) and our new data (Table 4) at room temperature. Hence, the differences in $D_{[100]}$ may stem from data processing and modeling, inaccuracies in temperature measurements, or could result from very slight misorientations of the single-crystal samples of Gibert et al. (2003a, 2005).

Comparison with other high-temperature data

Few reliable thermal diffusivity measurements for mantle olivine at high temperature are available due to the earlier mentioned problems associated with the various techniques and unwanted radiative transfer. Indeed, many older publications simply present results in graphs, do not tabulate their few actual measurements, and often ignore uncertainties in their methods. In Figure 11 we compare our laser-flash method data for the Needles samples to the measurements of Kobayashi (1974) and Gibert et al. (2005). These earlier studies access temperatures of up to ~900 °C and find that $D_{olivine}$ goes through a minimum before increasing slightly again toward the highest temperatures. Kanamori et al. (1968) and Lee and Kingery (1960) discussed upturns as being compatible with direct radiative transfer. Our olivine data clearly lack upturns (Fig. 11; see also Fig. 5 for pure forsterite and Co-doped forsterite at up to ~1500 °C). In fact, none of the minerals (garnet, quartz, olivine, spinels, Al_2O_3, MgO) studied in our laboratory so far show this peculiar behavior. This is likely to be an artifact of older methods that, among other problems, do not properly account for radiative transfer or suffer from contact losses (see earlier discussion). Nevertheless, there is reasonably good agreement between Gibert et al.'s (2003a, 2005) $D_{[010]}$ and $D_{[001]}$ and our data at temperatures of up to 200–300 °C. This indicates that their method can provide meaningful measurements for materials and conditions with insignificant radiative heat transfer.

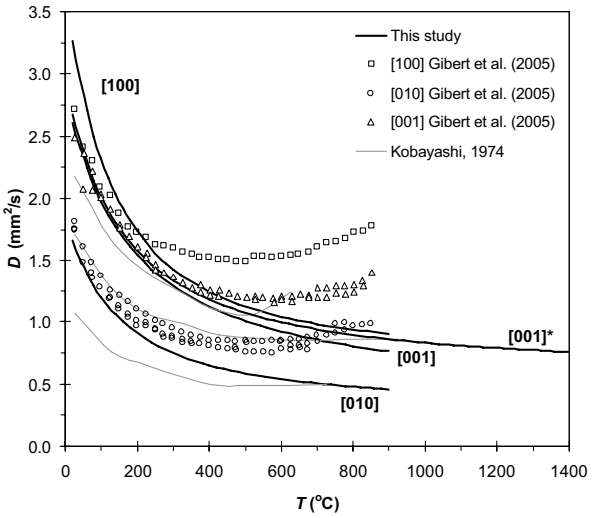

FIGURE 11. Comparison of our thermal diffusivity behavior at elevated temperature. Note the differences in room-temperature values between our data and those of Gibert et al. (2003a, 2005) and Kobayashi (1974). Also, the latter studies show that D goes through a minimum before increasing again at higher temperatures. Our new laser-flash method data clearly do not show this behavior, which we attribute to uncertainties in processing radiative transfer in the older methods of Kobayashi (1974) and Gibert et al. (2003a, 2005), see text for detailed discussion. Our data support the notion that thermal diffusivity becomes virtually independent of *T* at very high temperatures. The quartz and feldspar data of Höfer and Schilling (2002) also show the anomalous behavior.

Effect of chemical composition on thermal diffusivity of olivine

Cation substitution. Our variety of single-crystal samples provides information on the effect of composition on olivine and olivine-structured minerals. Previous studies (Kobayashi 1974; Chai et al. 1996; Gibert et al. 2003a, 2005; Osako et al. 2004; Xu et al. 2004) used olivine samples with a limited compositional range near Fo_{90}. In addition to such samples, we also analyzed several compositions with olivine structure (Table 1). Overall, $D_{[100]}$, $D_{[010]}$, and $D_{[001]}$ depend on molecular weight (Fig. 12) for the single crystals investigated here. Sinhalite and chrysoberyl have the lowest molecular weights and agree with the linear trends extrapolated from using just the forsterite, Co-doped forsterite, and mantle olivine data. Linear extrapolation of these trends provides estimates of the room temperature thermal diffusivities for more Fe-rich olivines with compositions of <Fo_{90}: near Fo_{70}, the [010] and [001] trends of olivine would intersect and have similar thermal diffusivities. However, this would result in unrealistic negative *D* values, hence it is likely that *D* becomes much less dependent on the Fe-content of olivine below Fo_{90}, resulting in a virtually constant D_{ol} for the more Fe-rich olivines.

Of the [001] orientations of the silicate samples at room temperature, pure forsterite has the highest observed *D* (5.15 mm^2/s). The substitution of a small amount of Co in olivine (0.3 wt% CoO) lowers *D* by ~20% (to 4.17 mm^2/s), see Table 2. The substitution of ~10% Fe for Mg in pure forsterite, as in typical mantle olivine, lowers *D* by ~50% for [001] (2.59 mm^2/s) when compared to pure forsterite. It appears that substitutions at trace

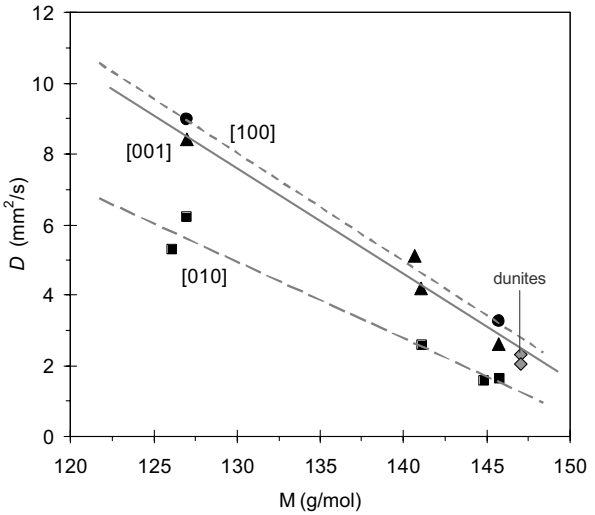

FIGURE 12. Thermal diffusivity of the [100], [010], and [001] orientations of olivine-group minerals as a function of molecular weight (as a proxy for composition). The sinhalite and chrysoberyl samples have the lowest molecular weights, compared to forsterite, Co-doped forsterite, and the mantle olivines. Overall, data seem to define linear trends for all three orientations, but we lacked Fe-rich single crystals to explore the more non-linear behavior at higher molecular weights.

or minor concentration levels have a much more pronounced effect in lowering *D* than substitutions at comparatively high concentrations and this effect is clearly non-linear. This also holds true for thermal diffusivity at high temperature: as can be seen in Figure 5, *D* values for Needles [001]* are 64% and 82% of the *D*-value for Co-doped forsterite [001] at room temperature and near 1400 °C, respectively. Therefore, this observation affirms our earlier statement that the slight differences in olivine compositions near Fo_{90}-Fo_{93} likely have no or little effect on measured *D* values; we also consider any effects of preferred partitioning of Mg between olivine M1 and M2 to be negligible at such high Fe concentrations. Unfortunately, we were unable to procure Fe-rich olivine single-crystal samples to further explore the non-linear nature of the effect of cation substitution of thermal diffusivity.

Effect of water in olivine. Data for the [010] orientations of the Needles and Sumput samples potentially allow estimation of the significance of water in thermal diffusivity of mantle olivine. At room temperature, the more H_2O-rich Needles olivine has a slightly higher *D* than the Sumput olivine (1.66 ± 0.04 and 1.59 ± 0.03 mm²/s, respectively, corresponding to 250 ± 50 and 60 ± 20 ppm H_2O by weight, respectively; Table 1). This is a relative difference in *D* of just 4%, but at high temperatures (~590 °C and above) the two samples have virtually identical thermal diffusivities of 0.54–0.56 mm²/s (Table 2). IR spectral characterization did not indicate that either olivine sample lost water during heating. It appears that differences in water content only cause very small changes in *D* of olivine at low temperatures, differences that may be difficult to distinguish within analytical uncertainty of *D*. At high mantle temperatures such differences may very well be insignificant, although this observation may be particular to olivine. A more thorough investigation of the effect of water on *D* and *k* for a variety of nominally anhydrous minerals (garnet, quartz) and some glasses is presented elsewhere (Hofmeister et al. 2006).

Polycrystalline samples and effect of secondary phases

Although not the primary focus of this paper, our thermal diffusivity data on olivine-bearing rocks nevertheless allows for important observations on the behavior of polycrystalline samples that contain minerals other than olivine. In the case of both dunite samples, *D* values of the rocks plot between $D_{[010]}$ and $D_{[001]}$ of the Needles mantle olivines (Fig. 9, see also Fig. 12). The average *D* of all three Needles olivine orientations is 2.5 mm²/s at room temperature, which should be representative of a polycrystalline olivine sample that has truly randomly oriented crystals. The dunites have room-temperature *D* values that are lower (2.3 and 2.05 mm²/s, respectively; see Table 2), indicating a larger contribution from the directions with lesser *D* ([010] and/or [001] orientations) to overall thermal diffusivity. The presence of small amounts of pyroxene minerals does not seem to affect thermal diffusivity of dunites to an extent that they are noticeably different from olivine single-crystal data of samples with similar chemistry. Despite the fact that they contain other minerals, the monticellite-, hortonolite-, and fayalite-bearing samples *all* follow the same form for temperature dependence of *D* that applies to single-crystal olivine group samples and dunites. Monticellite and hortonolite in our samples have molecular weights of 159 and 165 g/mol, heavier than typical mantle olivine, and therefore these samples are expected to have lower thermal diffusivity than the dunites (Figs. 9 and 12). The thermal diffusivity of the monticellite- and hortonolite-bearing samples is therefore either largely dominated by the olivine mineral in them, or, alternatively, the non-olivine minerals have similar molecular weights and/or significant concentrations of water or other cation substitutions that also lower thermal diffusivity. As can be seen in Figure 10, the monticellite-bearing sample is the only polycrystalline sample that has a thermal diffusivity trend that crosses the trend of any other polycrystalline sample, which we attribute to the presence of large amounts of epidote in this particular sample. The fayalite-bearing rock sample has overall higher *D* than the fayalite-bearing slag sample: the fayalite-bearing rock contains oxide minerals, which tend to have higher diffusivity values than structurally more complicated silicate minerals (e.g., Hofmeister 2001), thus contributing to the elevated *D*-value. In case of the fayalite-bearing slag sample, the presence of a quenched melt is the principal reason for the decreased *D*-value because glasses tend to have lower *D* than minerals of the same composition. For example, Lazard et al. (2003) obtain a room-temperature *D* for silica glass of ~0.8 mm²/s, whereas Höfer and Schilling (2002) report *D* values for the mineral quartz of 3.6–7 mm²/s, depending on the orientation of the crystal. Hence, the much lower diffusivity of glasses has a noticeable effect on the overall diffusivity of fayalite-bearing slag sample.

Functional form for $D(T)$ of the lattice component

At high temperatures (≥700 °C), D_{lat} of olivine-group minerals depends weakly on temperature (Figs. 4–10). The flat region occurs at temperatures roughly 50% larger than the Debye temperature (490 °C for forsterite; 460 °C for Fo_{90} olivine;

130 °C for fayalite; Anderson and Isaak 1995). The variation seen in D at room temperature observed among samples with different chemistry (and the same orientation) decreases with T (Figs. 6–8). Similarly, for a given composition, the differences in D among the three orientations decrease with T (Figs. 4 and 5, and similarly for chrysoberyl, Fig. 6). Apparently, dD/dT is correlated with D at 298 K. These traits lead to the flat region occurring at higher temperature for samples with large D at 298 K that generally have fewer impurity ions. Similar behavior was observed for diverse chemical compositions with the garnet structure (Hofmeister 2006) and is compatible with the DHO model (discussed above).

For olivine, $D(T)$ is best described by Equation 4, whereas for garnet it is Equation 3 that provides better fits (Hofmeister 2006). This difference is attributed to $\partial(\ln u)/\partial T$ being near –0.004 %/K for grossular and pyrope garnets but almost double for forsterite and olivine, –0.006 to –0.008 %/K (Anderson and Isaak 1995). Thus, garnet is better approximated by constant sound speeds than olivine. Data on FWHM of garnets are unknown, whereas $\partial(\ln \text{FWHM})/\partial T$ from Raman spectra of forsterite and olivine is ~0.14%/K (Kolesov and Geiger 2004a). The comparative large T derivative for the widths is compatible with the inverse temperature dependence of D (Eq. 3).

Thermal diffusivity of olivine and heat transport in Earth's mantle

As shown in Table 2 and in Figures 4–11, the thermal diffusivity of olivine becomes virtually independent of temperature at elevated temperatures. For typical mantle olivine compositions (our Needles and Sumput samples), D values are 0.79–0.87 mm^2/s at ~900–1000 °C for [001] and [100]. However, D of the [010] orientation is markedly lower with 0.51 mm^2/s at ~750 °C. The similarity between $D_{[100]}$ and $D_{[001]}$ makes it difficult to differentiate anisotropy in thermal diffusivity introduced from preferred orientations along the **a**- or **c**-axes of olivine. Hence, any significant anisotropy likely stems from a strong $D_{[010]}$ contribution because of the large differences in D values between [010] and the two other orientations. This agrees well with findings of anisotropy of thermal diffusivity in deformed dunite rocks (Gibert et al. 2003b): deformed olivine aggregates have the highest thermal diffusivity parallel to the lineation, dominated by $D_{[001]}$. Diffusivity normal to the foliation is lower due to the enhanced influence of $D_{[010]}$ in this plane.

Our results indicate that radiative heat transfer does play a role at elevated temperatures, for two completely different reasons. (1) As shown in Figure 3c, at high temperatures our data show a significant (~50% relative) radiative contribution to total thermal diffusivity in olivine, which was present in all orientations of all single crystals that we analyzed. Although this in fact constitutes boundary-to-boundary transport, and cannot be used to calculate diffusive radiative transfer, it shows that olivine is highly transparent to light at mantle temperatures. Specifically, it is transparent to the wavelengths of light that are produced at high temperatures (800–1200 °C) in our experiments. In addition, the mean free path in the experiments is close to the grain-size (d) of ~1 mm for the matrices of upper mantle rocks (Boyd and Meyer 1979) and this suggests that diffusive radiative transport will be high. For comparison, diffusive radiative transfer was recently calculated as a function of grain-size, based on spectroscopic measurements of olivine at temperature, and found to be 0.5 to 1.3 W/m-K from 1100 to 1600 °C, respectively, for d = 1 mm (Hofmeister 2005). The calculated value for k_{rad} is a significant fraction of the asymptotic value of ~3.0 W/m-K for Fo_{92}, averaged for the three directions of olivine at 800 °C, and is roughly similar to the direct component in our experiments. We used tabulated values of $\rho(T)$ for Fo_{90} (Anderson and Isaak 1995) and the heat capacities for olivine were obtained using the formulation of Berman and Brown (1985). (2) More importantly, the temperature dependence of k critically affects convection through non-linear terms in the temperature equation that governs mantle convection (e.g., Dubuffet et al. 1999, 2000, 2002; Yuen et al. 2000). The mathematical form taken by the temperature equation is the key reason that $\partial k/\partial T$ is important. If k is constant, the temperature equation is a relatively simple and linear partial differential equation, if k depends on T, the temperature equation can become extremely non-linear in temperature. Different classes of solutions are obtained for constant and variable k from the temperature equation (e.g., Barenblatt 1996). Specifically, k_{rad} increasing with T controls the time dependence and stabilizes the planforms of mantle convection through positive feedback (Dubuffet et al. 2002). Because feedback is lacking for constant k or D (the phonon contribution at high temperature), the diffusive radiative transfer controls the outcome of mantle convection calculations and thus should be the key process inside the mantle. For conductive parts of the mantle the phonon contribution remains important, particularly in the colder regions, such as the subducting slabs (high k_{lat}), but *both* mechanisms must be considered. We therefore conclude that heat transfer by *photons* does indeed play a significant role in Earth's upper mantle, though it may play a subordinate role to the role of *phonons* in the colder continental and oceanic crusts.

Acknowledgments

We thank G. Benedix for help in the electron microprobe laboratory at Washington University and C. Lundstrom for access to the SEM at the University of Illinois. We also thank B. Gibert and F. Schilling for their reviews. This publication is supported by NSF grant EAR-0207198 to AMH.

References cited

Anderson, O.L. and Isaak, D.G. (1995) Elastic constants of mantle minerals at high temperature. In T.J. Ahrens, Ed., Handbook of Physical Constants, p. 64–96. American Geophysical Union, Washington, D.C.

Barenblatt, G.I. (1996) Scaling, Self-Similarity, and Intermediate Asymptotics. Cambridge University Press, Cambridge.

Bauerhansl, P. and Beran, A. (1997) Trace hydrogen in the olivine-type minerals chrysoberyl, Al_2BeO_4 and sinhalite, $MgAlBO_4$—a polarized FTIR spectroscopic study. Schweizerische Mineralogische und Petrographische Mitteilungen, 77, 131–136.

Beck, A.E., Darbha, D.M., and Schloessin, H.H. (1978) Lattice conductivities of single-crystal and polycrystalline materials at mantle pressures and temperatures. Physics of the Earth and Planetary Interiors, 17, 35–53.

Bell, D.R., Rossman, G.R., Maldener, J., Endisch, D., and Rauch, F. (2003) Hydroxide in olivine: a quantitative determination of the absolute amount and calibration of the IR spectrum. Journal of Geophysical Research, 108, 2105, doi: 10.1029/2001JB000679.

Berman, R.G. and Brown, T.H. (1985) Heat capacity of minerals in the system Na_2O–K_2O–CaO–MgO–FeO–Fe_2O_3–Al_2O_3–SiO_2–TiO_2–H_2O–CO_2: representation, estimation, and high temperature extrapolation. Contributions to Mineralogy and Petrology, 89, 168–183.

Blumm, J. and Lemarchand, S. (2002) Influence of test conditions on the accuracy of laser flash measurements. High Temperatures–High pressures, 34, 523–528.

Blumm, J. and Opfermann, J. (2002) Improvement of the mathematical modeling of flash measurements. High Temperatures–High pressures, 34, 515–521.

Blumm, J., Henderson, J.B., Nilson, O., and Fricke, J. (1997) Laser flash measurement of the phononic thermal diffusivity of glasses in presence of ballistic radiative transfer.

High Temperatures-High Pressures, 29, 555–560.
Boyd, F.R. and Meyer, H.O.A. (1979) The mantle sample: Inclusions in kimberlites and other volcanics, Proceedings of the second international kimberlite conference, Vol. 2, American Geophysical Union, Washington D.C.
Branlund, J.M. and Hofmeister, A.M. (2004) Effects of hydrogen impurities on the lattice thermal diffusivity of quartz and quartzites up to 1000°C. Eos, Transactions, AGU, 85(47), Fall Meeting Supplement, Abstract.
Branlund, J.M., Kameyama, M.C., Yuen, D.A., and Kaneda, Y. (2000) Effects of temperature-dependent thermal diffusivity on shear instability in a viscoelastic zone: implications for faster ductile faulting and earthquakes in the spinel stability field. Earth and Planetary Science Letters, 182, 171–185.
Bräuer, H., Dusza, L., and Schulz, B. (1992) New laser flash equipment LFA 427. Interceram, 41, 489-492.
Buettner, R., Zimanowski, B., Blumm, J., and Hagemann, L. (1998) Thermal conductivity of a volcanic rock material (olivine–melilitite) in the temperature range between 288 and 1470 K. Journal of Volcanology and Geothermal Research, 80, 293–302.
Burns, R.G. (1970) Mineralogical Applications of Crystal Field Theory. Cambridge University Press, U.K.
Chai, M., Brown, J.M., and Slutsky, L.J. (1996) Thermal diffusivity of mantle minerals. Physics and Chemistry of Minerals, 23, 470–475.
Clark, S.P., Jr. (1957) Radiative transfer in the Earth's mantle. Transactions, American Geophysical Union, 38, 931–938.
Cowen, D.R. (1963) Pulse method of measuring thermal diffusivity at high temperatures. Journal of Applied Physics, 34, 926–927.
Debye, P. (1914) Vorträge über die kinetische Theorie der Materie und der Elektrizität. B.G. Teuber, Berlin.
Degiovanni, A., Andre, S., and Maillet, D. (1994) Phonic conductivity measurement of a semi-transparent material. In T.W. Tong, Ed., Thermal conductivity, 22, p. 623–633. Technomic, Lancaster, Pennsylvania.
Dubuffet, F., Yuen, D.A., and Rabinovicz, M. (1999) Effects of a realistic mantle thermal conductivity on the patterns of 3D convection. Earth and Planetary Science Letters, 171, 401–409.
Dubuffet, F., Yuen, D.A., and Yanagawa, T.K. (2000) Feedback effects of variable thermal conductivity on cold downwellings in high Rayleigh number convection. Geophysical Research Letters, 27, 2981–2984.
Dubuffet, F., Yuen, D.A., and Rainey, E.S.G. (2002) Controlling thermal chaos in the mantle by positive feedback from radiative thermal conductivity. Nonlinear Processes in Geophysics, 9, 1–13.
Farrell, E.F. and Newnham, R.E. (1965) Crystal-field spectra of chrysoberyl, alexandrite, peridot, and sinhalite. American Mineralogist, 50, 1972–1981.
Gibert, B., Schilling, F.R., Tommasi, A., and Mainprice, D. (2003a) Thermal diffusivity of olivine single-crystals and polycrystalline aggregates at ambient conditions—a comparison. Geophysical Research Letters, vol. 30, no. 22, doi:10.1029/2003GL018459.
Gibert, B., Seipold, U., Tommasi, A., and Mainprice, D. (2003b) Thermal diffusivity of upper mantle rocks: influence of temperature, pressure and the deformation fabric. Journal of Geophysical Research, 108(B8), doi:10.1029/2002JB002108.
Gibert, B., Schilling, F.R., Gratz, K., and Tommasi, A. (2005) Thermal diffusivity of olivine single crystals and a dunite at high temperature: Evidence for heat transfer by radiation in the upper mantle. Physics of the Earth and Planetary Interiors, 151, 129–141.
Giesting P.A. and Hofmeister A.M. (2002) Thermal conductivity of disordered garnets from infrared spectroscopy. Physical Review, B65, paper 144305.
Hauck, S.A., Phillips, R.J., and Hofmeister, A.M. (1999) Variable conductivity: effects on the thermal structure of subducting slabs. Geophysical Research Letters, 26, 3257–3260.
Henderson, J.B., Giblin, F., Blumm, J., and Hagemann, L. (1998) SRM 1460 series as a thermal diffusivity standard for laser flash instruments. International Journal of Thermophysics, 19, 1647–1656.
Höfer, M. and Schilling, F.R. (2002) Heat transfer in quartz, orthoclase, and sanidine at elevated temperature. Physics and Chemistry of Minerals, 29, 571–584.
Hofmeister, A.M. (1999) Mantle values of thermal conductivity and the geotherm from phonon lifetimes. Science, 283, 1699–1706.
——— (2001) Thermal conductivity of spinels and olivines from vibrational spectroscopy at ambient conditions. American Mineralogist, 86, 1188–1208.
——— (2004) Thermal conductivity and thermodynamic properties from infrared spectroscopy. In P. King, M. Ramsey, and G. Swayze, Eds., Infrared Spectroscopy in Geochemistry, Exploration Geochemistry, and Remote Sensing, p. 135–154. Mineralogical Association of Canada, Ottawa, Ontario.
——— (2005) The dependence of radiative transfer on grain-size, temperature, and pressure: implications for mantle processes. Journal of Geodynamics, 40, 51–72.
——— (2006) Thermal diffusivity of garnets at high temperature. Physics and Chemistry of Minerals, 33, 45–62, DOI: 10.1007/s00269-005-0056-8.
Hofmeister, A.M. and Mao, H.K. (2001) Evaluation of shear moduli and other properties of silicate spinels from IR spectroscopy. American Mineralogist, 86, 622–639.
Hofmeister, A.M., Pertermann, M., Branlund, J.M., and Whittington, A.G. (2006) Geophysical implications of reduction in thermal conductivity due to hydration. Geophysical Research Letters, 33, L11310, DOI: 10.1029/2006GL026036.
Honda, S. and Yuen, D.A. (2001) Interplay of variable thermal conductivity and expansivity on the thermal structure of oceanic lithosphere. Geophysical Research Letters, 28, 351–354.
Kanamori, H., Fujii, N., and Mizutani, H. (1968) Thermal diffusivity of rock-forming minerals. Journal of Geophysical Research, 73, 595–605.
Katsura, T. (1995) Thermal diffusivity of olivine under upper mantle conditions. Geophysical Journal International, 122, 63–69.
Kobayashi, Y. (1974) Anisotropy of thermal diffusivity in olivine, pyroxene and dunite. Journal of Physics of the Earth, 22, 359–373.
Kolesov, B.A. and Geiger, C.A. (2004a) A Raman spectroscopic study of Fe-Mg olivines. Physics and Chemistry of Minerals, 31, 142–154.
——— (2004b) A temperature-dependent single-crystal Raman spectroscopic study of fayalite: evidence for phonon-magnetic excitation coupling. Physics and Chemistry of Minerals, 31, 155–161.
Lazard, M., Andre, S., and Maillet, D. (2003) Thermal characterization of semi-transparent media: measurement of phononic diffusivity of glass and silica. European Journal of Physics, Applied Physics, 23, 207–211, DOI 10.1051/epjap:200320.
Lee, D.W. and Kingery, W.D. (1960) Radiation energy transfer and thermal conductivity of ceramics and oxides. Journal of the American Ceramic Society, 43, 594–607.
Mehling, H., Hautzinger, G., Nilsson, O., Fricke, J., Hofmann, R., and Hahn, O. (1998) Thermal diffusivity of semitransparent materials determined by the laser-flash method applying a new mathematical model. International Journal of Thermophysics, 19, 941–949.
Mitra, S.S. (1969) Infrared and Raman spectra due to lattice vibrations. In S. Nudelman and S.S. Mitra, Eds., Optical Properties of Solids, p. 333–452. Plenum Press, New York.
Miyake, M., Nakamura, H., Kojima, H., and Marumo, F. (1987) Cation ordering in Co-Mg olivine solid-solution series. American Mineralogist, 72, 594–598.
Monaghan, B.J. and Quested, P.N. (2001) Thermal diffusivity of iron at high temperature in both the liquid and solid states. The Iron and Steel Institute of Japan International, 41, 1524–1528.
Osako, M., Ito, E., and Yoneda, A. (2004) Simultaneous measurements of thermal conductivity and thermal diffusivity for garnet and olivine under high pressure. Physics of the Earth and Planetary Interiors, 143–144, 311–20.
Parker, J.W., Jenkins, J.R., Butler, P.C., and Abbott, G.I. (1961) Flash method of determining thermal diffusivity, heat capacity, and thermal conductivity. Journal of Applied Physics, 32, 1679–1684.
Reif, F. (1965) Fundamentals of Statistical and Thermal Physics. McGraw Hill, New York.
Ross, R.G., Andersson, P., Sundqvist, B., and Bäckström, G. (1984) Thermal conductivity of solids and liquids under pressure. Reports on Progress in Physics, 47, 1347–1402.
Scalvi, R.M.F., Li, M.S., and Scali, L.V.A. (2003) Annealing effects on optical properties of natural alexandrite. Journal of Physics: Condensed Matter, 15, 7437–7443.
Schilling, F.R. (1999) A transient technique to measure thermal diffusivity at elevated temperature. European Journal of Mineralogy, 11, 1115–1124.
Seipold, U. (1998) Temperature dependence of thermal transport properties of crystalline rocks—a general law. Tectonophysics, 291, 161–171.
Shankland, T.J. and Hemmenway, K. (1965) Synthesis of forsterite crystals. American Mineralogist, 48, 200.
Shankland, T.J., Nitsan, U., and Duba, A.G. (1979) Optical absorption and radiative heat transport in olivine at high temperature. Journal of Geophysical Research, 84, 1603–1610.
Slack, G. (1964) Thermal conductivity of pure and impure silicon, silicon carbide, and diamond. Journal of Applied Physics, 35, 3460–3466.
Taran, M.N. and Langer, K. (2001) Electronic absorption spectra of Fe^{2+} ions in oxygen-based rock-forming minerals at temperatures between 297 and 600 K. Physics and Chemistry of Minerals, 28, 199–210.
Taran, M.N. and Rossman, G.R. (2001) Optical spectra of Co^{2+} in three synthetic silicate minerals. American Mineralogist, 86, 889–895.
Ullrich, K., Langer, K., and Becker, K.D. (2002) Temperature dependence of the polarized electronic absorption spectra of olivines. Part I—fayalite, Physics and Chemistry of Minerals, 29, 409–419.
Ullrich, K., Ott, O., Langer, K., and Becker, K.D. (2004) Temperature dependence of the polarized electronic absorption spectra of olivines. Part II–cobalt-containing olivines. Physics and Chemistry of Minerals, 31, 247–260.
Van Den Berg, A.P., Yuen, D.A., and Allwardt, J.R. (2002) Non-linear effects from variable thermal conductivity and mantle internal heating: implications for massive melting and secular cooling of the mantle. Physics of the Earth and Planetary Interiors, 129, 359–375.
Xu, Y., Shankland, T.J., Linhardt, S., Rubie, D.C., Langenhorst, F., and Klasinski, K. (2004) Thermal diffusivity and conductivity of olivine, wadsleyite, and ringwoodite to 20 GPa and 1373 K. Physics of the Earth and Planetary Interiors, 143–144, 321–326.
Yuen, D.A., Vincent, A.P., Bergeron, S.Y., Dubuffet, F., Ten, A.A., Steinbach, V.C., and Starin, L. (2000) Crossing of scales and nonlinearities in geophysical processes, In E. Boschi, G. Ekstrom, and A. Morelli, Eds., Problems in Geophysics for the New Millenium, p. 405–465. Editrice Compositori, Bologna, Italy.

MANUSCRIPT RECEIVED SEPTEMBER 27, 2005
MANUSCRIPT ACCEPTED JUNE 17, 2006
MANUSCRIPT HANDLED BY DAN SHIM